# Synthesis and characterization of silver–carbon nanoparticles produced by high-current pulsed arc

F. Maya, S. muhl, O. Peña, M. Miki-Yoshida

## Abstract

In this paper, we report the formation of silver–carbon encapsulated metal nanoparticles (EMN's) using a high-current pulsed arc system in an argon atmosphere. The deposits were studied by Optical Extinction Spectroscopy (OES), X-ray diffraction (XRD) and Transmission Electron Microscopy (TEM); the chemical analysis of the deposits was performed using Energy Dispersion X-ray spectroscopy (EDX). Using the total nanoparticle diameter, the bulk crystalline density of silver and an estimate amorphous carbon (a-C) density we have calculated the size of the silver nucleus and the thickness of the a-C coating as a function of the argon gas pressure. The OES spectra of the EMN's exhibited two peaks characteristic of the Surface Plasmon Resonance (SPR) of elongated/very close silver nanoparticles; a subsequent thermal annealing strongly increased the SPR peaks. The double peak SPR spectra were modeled using calculations based on the existence of silver nanoparticles in the form of prolate spheroids. The main advantage of our preparation method is that the metal nanoparticles are encapsulated in a-C from the beginning and this layer acts as an efficient chemical barrier.

Keywords: Arc evaporation, High current, Silver nanoparticles, Surface plasmon resonance.

## Introduction

The discovery of the formation of diverse nanostructured forms of carbon by the Kratschmer-Huffman carbon arc method and the modifications developed by Dravid have together generated a strong interest in the production of nanostructured materials for many applications. Such techniques have been used to produce not only carbonaceous materials but also a wide range of encapsulated metal nanoparticles (EMN's) using DC continuous arcs, of around 100 A in He, Ar or H at 26.7–66.5 kPa. However, there are a few reports of the advantages of using pulsed arcs in the same current range but the formation process of the clusters and nanoparticles is not fully understood. The interest in core–shell nanostructured materials arises from the fact that their intrinsic properties can be easily tuned by changing either their relative size [1] or the composition of both core and shell [2]. For example, both nanoshells (a dielectric core surrounded by a metallic shell) and nanocables (nanowires encapsuled in various kind of nanotubes) have been widely investigated recently [3–6].

One of the more interesting of such core–shell systems is composed of Ag nanoparticles encapsulated by crystalline or amorphous carbon. Silver exhibits outstanding optical properties and excellent thermal and electrical conductivity and therefore has been extensively used in catalysis, electronics, photonics, photography, biological labeling, surface-enhanced Raman scattering and optical devices [7–10]. However, these nanoparticles readily oxidize in air and have a poor biocompatibility; nevertheless, if a carbon shell is added both problems are solved and the range of prospective applications is increased. Based on this strategy, composite nanostructures using nanoscale silver as the core and carbon as the shell have been prepared by some groups. For example, Ag/C nanocables and Ag/C nanoparticles have been synthesized

in the presence of PVP [11] and silver/crosslinked poly (vinyl alcohol) coaxial nanocables have been prepared [12].

In this work we have used High-current Pulsed electric arcs in Argon ambient between graphite ($3.3\times10^{-3}$ m of diameter) and silver ($1.5\times10^{-3}$ m of diameter) electrodes to produce silver–carbon nanoparticles. The resulting nanoparticles were analyzed by Transmission Electron Microscopy (TEM), Scanning Electron Microscopy (SEM), Optical Extinction Spectroscopy (OES) and X-Ray Diffraction (XRD). The composition of the thin films was analyzed using energy dispersive X-ray spectroscopy (EDS) in a Cambridge-Leica, Mod. Stereoscan 440 Scanning Electron Microscopy, with an OXFORD Pentafet EDS detector.

There are various modeling approaches for the analysis of the OES data. In a previous study we have found that the T-Matrix method outlined below gives satisfactory results [13].

Matrix method:

The T-Matrix method was originally developed by Waterman [14] and later improved byMishchenko et al. [15–17]. The general idea of this method is to expand the incident and scattered fields, $E\overrightarrow{inc}$ and $E\overrightarrow{sca}$, in terms of appropriate sets of vector spherical harmonics $M\overrightarrow{mn}$, $N\overrightarrow{mn}$ [18]:

$$\overrightarrow{E_{inc}}(k\overrightarrow{r}) = E_0 \sum_{n=1}^{\infty} \sum_{m=-n}^{n} Rg[a_{mn}\overrightarrow{M}_{mn}(k\overrightarrow{r}) + b_{mn}\overrightarrow{N}_{mn}(k\overrightarrow{r})] \quad (1)$$

$$\overrightarrow{E_{sca}}(k\overrightarrow{r}) = E_0 \sum_{n=1}^{\infty} \sum_{m=-n}^{n} [p_{mn}\overrightarrow{M}_{mn}(k\overrightarrow{r}) + q_{mn}\overrightarrow{N}_{mn}(k\overrightarrow{r})], \quad (2)$$

where $E_0$ is the amplitude of the incident field, Rg is a normalization constant, $a_{mn}$ and $b_{mn}$ are the expansion coefficients,which are assumed to be known, and for an incident plane wave, are expressed in terms of associated Legendre functions and their derivatives [14] where $p_{mn}$ and $q_{mn}$ are the expansion coefficients characterizing the scattered field. These are obtained by multiplying the known expansion coefficients of the incident field by means of a so-called transition matrix or T-matrix:

$$\begin{bmatrix} p_{mn} \\ q_{mn} \end{bmatrix} = [T-matrix] \begin{bmatrix} a_{mn} \\ b_{mn} \end{bmatrix} = \begin{bmatrix} T^{11} & T^{12} \\ T^{21} & T^{22} \end{bmatrix} \begin{bmatrix} a_{mn} \\ b_{mn} \end{bmatrix}. \quad (3)$$

The T-matrix elements depend on the particle's size, shape, composition and orientation, but not on the nature of the incident or scattered fields. Now, expressions can be found to calculate the extinction and scattering cross sections from the T-matrix elements [18]:

$$\sigma_{ext} = \frac{2\pi}{k^2} \mathrm{Re} \left( \sum_{n=1}^{\infty} \sum_{m=-n}^{n} T^{11}_{mnm'} + T^{22}_{mnm'} \right) \quad (4)$$

$$\sigma_{sca} = \frac{2\pi}{k^2} \sum_{i,j=1}^{2} \sum_{n=1}^{\infty} \sum_{n'=1}^{\infty} \sum_{m=0}^{\min(n,n')} (2-\delta_{m0}) \left| T^{ij}_{mnn'} \right|^2. \quad (5)$$

Finally, before comparing the experimental results and the simulations, it is necessary to compute the optical density. The procedure is relatively straightforward and will not be described here; a detailed discussion has been offered, for example, in Ref. [19].

**Experiment**

The experimental apparatus is described in detail elsewhere [20,21]. For the metal carbon work, $3.12\times10^{-3}$ m diameter high purity AERO graphite from ESPI and $1.5\times10^{-3}$ m of diameter silver wire (99.9% purity) were used as the electrodes. The maximum arc current and its temporal form were sensed by measuring the voltage drop across a low inductance 0.98 mW resistor in the arc circuit, connected to a HP54522A Digital oscilloscope. The arc was generated in argon (99.99% purity) at pressures of 13 to 106 kPa and a 0.40 m diameter piece of glass tubing surrounding the electrodes was used to collect the deposit. For the TEM analysis, the deposit was removed from the inside of the tube by agitation in methanol using an ultrasonic bath. Drops of this liquid were then applied to a TEM grid coated with a holey polymer layer or for the SEM analysis the liquid was applied to a piece of high purity n type silicon wafer. The deposits were also characterised by X-ray diffraction, SEM and EDX. The composition of the samples was measured in an area of at least 5 μm2.

Optical extinction spectra were obtained at room temperature using a Cary 500 double-beam spectrophotometer in the 330–800 nm wavelength range, before and after the thermal annealing, in order to detect the existence of the Surface Plasmon Resonance, indicative of the presence of silver nanoparticles. For these measurements the nanoparticles were deposited on a soda lime substrate and a thermal treatment was applied at 400 °C for one hour in an Argon atmosphere. The experimental OES spectrawere comparedwith calculations of the optical density performed using the T-Matrix method [22], in order to find the parameters which provided the best fit. The bulk

dielectric function values reported by Johnson and Christy [23] were used for the calculations, after applying a correction to incorporate surface dispersion effects [1].

**Results**

Fig. 1 shows that the maximum arc current linearly decreased as the argon gas pressure was increased from 13 to 106 kPa. The insert in Fig. 1 shows the temporal variation of the arc current; the FWHM duration of the arc is approximately 25 ms. Similar results of both the temporal variation of the arc current and the maximum arc current versus gas pressure, althoughwith large valueswere observed using helium. Fig. 2a is a TEMmicrograph of a nanoparticle prepared using an argon pressure of 40 kPa the crystalline silver nucleus andamorphous carbon coat canbe clearly seen. More than 20 different sized nanoparticles were studied by tem and the carbon layer was always amorphous. The a-C layerwas seen to be a very effective chemical barrier since no reaction was detected when nanoparticles were added to concentrated hydrochloric acid.

The left-hand side axis of Fig. 3 shows the average particle radius of the deposits prepared at the different pressures. This average radius was obtained from the measurements of at least 40 particles in SEM micrographs of the deposits. The average composition of the samples was measured over an area which included the 40 nanoparticles, only Ag, C, Si and O were detected (measurement of the silicon substrate without nanoparticles showed that the oxygen signal was from the native SiOx layer). Fig. 2b is a SEM micrograph of silver nanoparticles prepared at an argon pressure of 66 kPa, even though the micrograph shows less than the 50 nanoparticless referred to the selection gives a good idea of the distribution of sizes. Our earlier work

[21] and theTEM analysis of the present deposits demonstrated that the nanoparticles consist of a small crystalline metal nucleus cover by an amorphous carbon layer. If we assume that the particle is spherical then:

$$\frac{m_C}{m_{Ag}} = \frac{\rho_C}{\rho_{Ag}} * \frac{r_{np}^3 - r_{Ag}^3}{r_{Ag}^3} \quad (6)$$

Where $m_C$ and $m_{Ag}$ are themass of carbon and silver in the nanoparticle, $\rho_C$ and $\rho_{Ag}$ are the densities of carbon and silver, $r_{np}$ and $r_{Ag}$ are the radii of the nanoparticle and the silver nucleus. This can be rearranged to give:

$$r_{Ag} = \frac{r_{np}}{\sqrt[3]{\frac{m_C}{m_{Ag}} * \frac{\rho_{Ag}}{\rho_C} + 1.}} \quad (7)$$

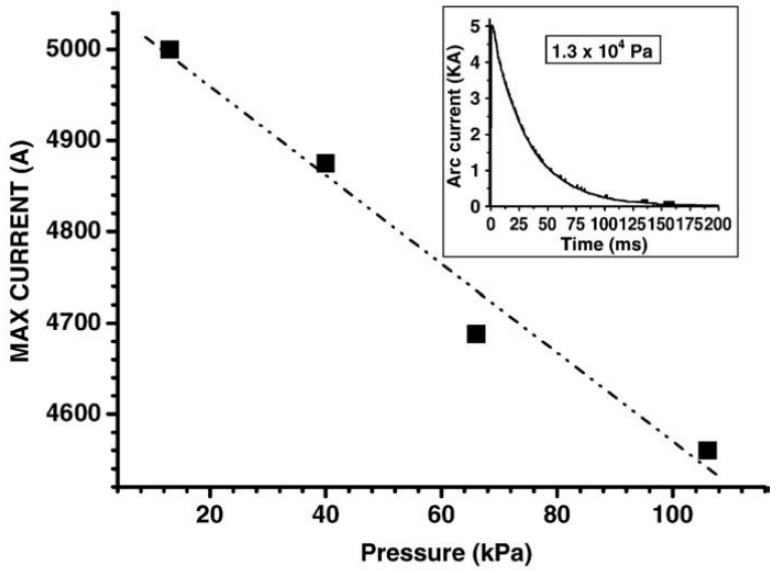


**Fig. 1.** The measured maximum of the arc current as a function of the argon gas pressure. The insert shows the temporal variation of the arc current for a gas pressure of 13 kPa.

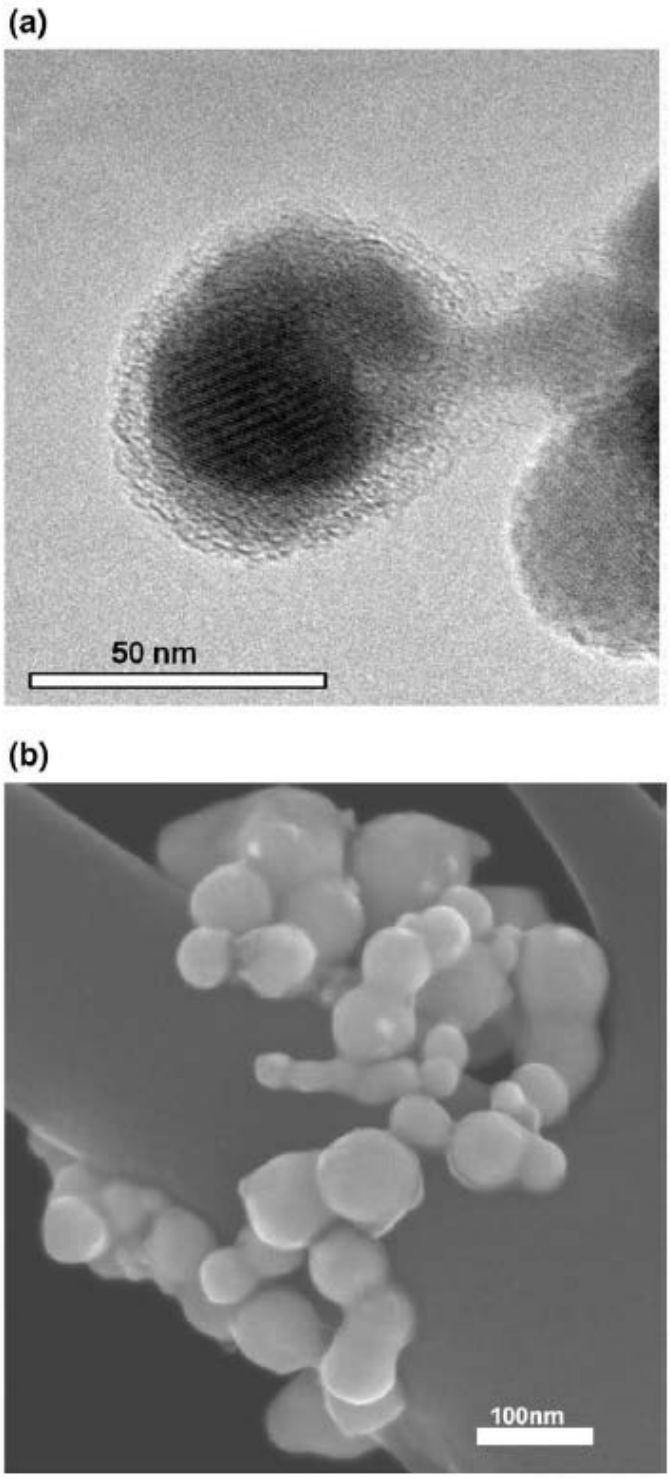


**Fig. 2.** a. A TEM micrograph of a silver nanoparticle prepared in 40 kPa of argon. b. A SEM micrograph of silver nanoparticles prepared in 66 kPa of argon.

Using the bulk density of silver, 10.5 g/cm$^3$, and an estimated amorphous carbon density of 1.8 g/cm$^3$ [24], together with the C to Ag mass ratio of the deposit calculated from the EDX measured composition (ignoring the signal from Si and O), see table 1, it was possible to estimate the radius of the silver nucleus and the thickness of the a-C layer in the nanoparticle. The variation of the radius of the nucleus and layer thickness with argon gas pressure is plotted in Fig. 3 against the right-hand axis. For the range of pressures studied, the nanoparticle radius, the nucleus radius and the layer thickness increased linearly with the gas pressure ($R \geq 0.98$). Fig. 4 shows a typical XRD spectrum from the deposits clearly demonstrating the crystallinity of the silver nucleus. No peaks associated with graphite were observed. Table 1 lists the grain size obtained by a Scherrer analysis of the 111 XRD peaks, together with the sizes calculated from the mass ratio as outlined above and the particle size obtained from the modelling of the OES spectra [25]. The radius of the nucleus obtained from the XRD data and the mass ratio/density analysis was very similar for the lowest pressures but the XRD value was approximately double that of the mass ratio calculated value for the highest pressure. The grain size values from the SPR modelling were consistently smaller than the other values except for the lowest pressure. However, the tendency of the grain size versus the gas pressure was the same in all cases.

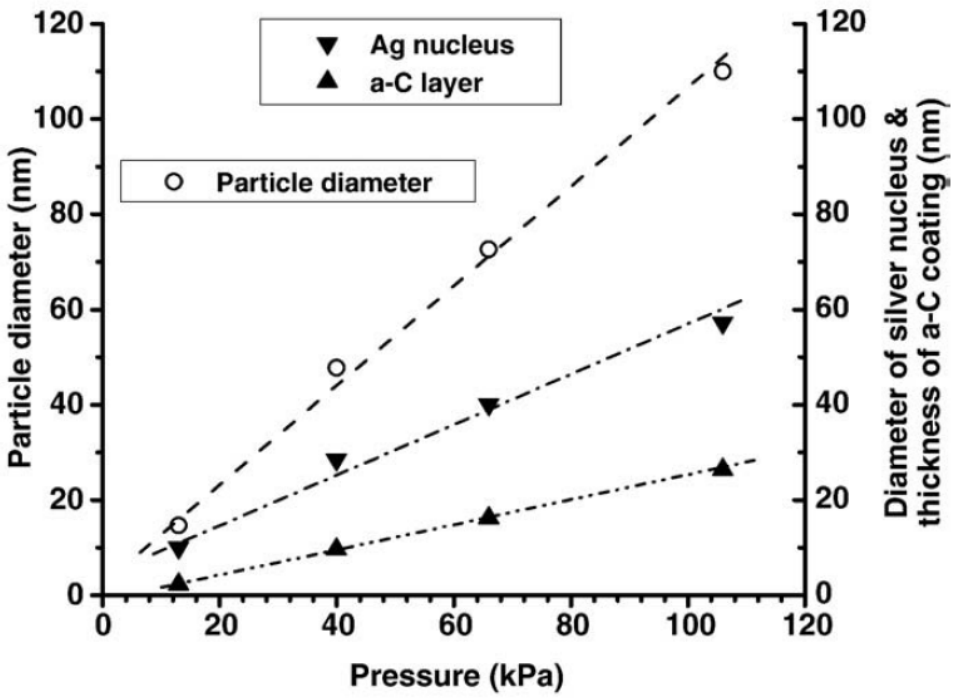


**Fig. 3.** The left hand side axis shows the measured nanoparticle radius versus the argon gas pressure. The right hand side axis shows the calculated radius of the silver nucleus and the a-C coating.

The optical response before the thermal annealing (not shown) presented little indication of the Surface Plasmon Resonance which probably meant that the carbon layer was too thick and masked the silver signal. After the annealing, a clear two-peak silver SPR signal appeared in all cases, which could be reasonably fitted using calculations based on the T-Matrix method for prolate spheroids (the shape formed by rotating an ellipse around its major axis), see Fig. 5. The prolate spheroids can be described by using two parameters: b, which is the rotational (transversal) semi-axis, and a, the longitudinal semi-axis; but often it is more convenient to describe their shape using the aspect ratio $\varepsilon=a/b$ and their size using the radius rV of a sphere having the same volume. The legends of the graphs shown in Fig. 5 contains the values of the

equivalent radius, $r_v$, the aspect ratio, ε, the standard deviation, σε, of ε and the areal density of silver, ϕ, in atoms/cm$^2$ used in the modeling of each of the spectra.

## Discussion

The observed decrease in arc current with increasing gas pressure is somewhat difficult to explain but it is probably associated with a

**Table 1**
The composition of the nanoparticles, expressed as percentage mass of silver and carbon, and the crystalline grain size of the silver nucleus of the nanoparticles calculated from the FWHM of the peaks measured by X-ray diffraction and the carbon to silver mass ratio, both as a function of the argon gas pressure.

| Pressure (kPa) | % mass of carbon (mC) | % mass of silver (mAg) | Ratio of the mass of carbon to silver (mC/mAg) | Grain size of the silver crystal (nm) | | |
|---|---|---|---|---|---|---|
| | | | | XRD | Calculated | SPR |
| 13 | 32.36 | 67.64 | 0.48 | 10.7 | 10.0 | 9.8 |
| 40 | 44.73 | 55.27 | 0.81 | 27.9 | 28.5 | 12 |
| 66 | 52.02 | 47.98 | 1.08 | 58.6 | 40.1 | 15 |
| 106 | 57.22 | 42.78 | 1.34 | 91.1 | 57.2 | 20 |

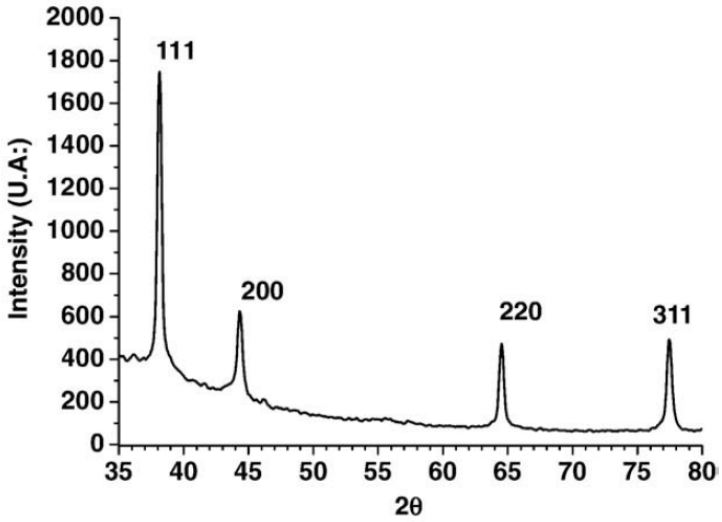


**Fig. 4.** A typical X-ray diffraction spectrum of the nanoparticles.

confinement of the arc plasma due a larger number of collisions between the vaporized carbon and the surrounding argon gas. We intend to study the temporal and spatial development of the arc using rapid photography and will report the results in the near future.

The form and separation of the two SPR peaks shows that they are not merely an effect of size (resonances of higher order) [26]. Several particle shapes were tried to adjust the OES spectra but the best fit was obtained for spheroidal particles, assuming a single equivalent radius $r_V$ and a Gaussian distribution of aspect ratios, with mean values $\varepsilon$ and standard deviation $\sigma_\varepsilon$. Nevertheless, in the TEM images, mainly quasispherical NPs are observed, which leads us to believe that probably the two peaks are an effect due to the short distance between neighboring particles rather than a real deformation. This is reinforced by the fact that the best fit is obtained for nanospheroids with an aspect ratio very close to 2.0, which have an optical response very similar to two touching spheres [27,28]. The case where the worse fit is obtained (40 kPa) is precisely where the lower wavelength peak is weaker and the other one wider (and the aspect ratio obtained from the fit is considerably smaller than in the other cases), showing that probably there are more complex size/shape/distance distributions which are hard to simulate by means of the simple model employed. Anyway, the results are very interesting because the presence of the SPR in carboncoated silver nanoparticles shows that it is possible to use them in optical applications where biocompatibility and/or protection from the medium are required.

As was noted before, there is a difference in the radii determined by the three different methods. Those discrepancies are probably related to the group of particles

sensed by each technique: the XRD grain size is an average value somewhat weighted towards the larger mass nanoparticles, the EDX size is based on a somewhat truer average since the compositional information was collected over an area of various square microns, and finally, the Optical Extinction only registered those nanoparticles that had a carbon layer sufficiently thin to allow the detection of the Ag SPR and was therefore based towards the smaller particles.

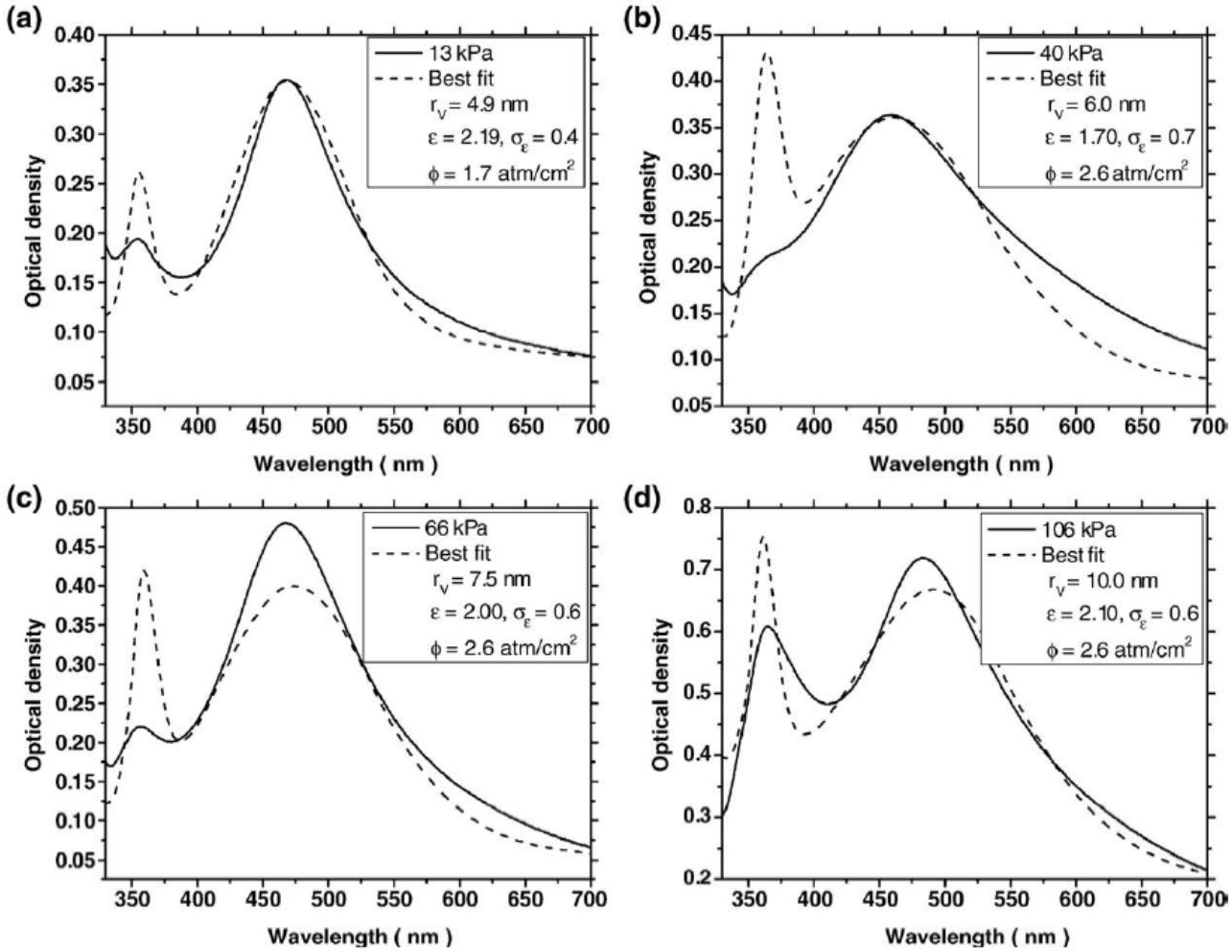


**Fig. 5.** Best fits of the OES spectra for 13 (a), 40 (b), 66 (c) and 106 kPa (d), showing the experimental spectra (continuous lines) and the simulated ones (dotted lines) for the given values of equivalent radius ($r_V$), aspect ratio ($\varepsilon$), aspect ratio dispersion ($\sigma_\varepsilon$) and areal density of silver, $\phi$. All samples were annealed at 400 °C in argon.

## Conclusions

In this work we have produced and characterized encapsulated silver nanoparticles produced by high-current pulsed electric arcs in an Ar atmosphere. The resulting NPs consist of a crystalline silver nucleus coated with amorphous carbon. It was found that the deposition rate increased when the gas pressure was decreased. The size of the silver nucleus and the thickness of the amorphous carbon coating were found to increase with increasing gas pressure, and that the rate of increase in the nucleus size was somewhat greater than that of the coating. The NPs could be collected either as a colloidal suspension or as a pseudo thin film. Additionally, it was found that by applying a thermal annealing the SPR signal could be considerably enhanced.

## Acknowledgements

The authors wish to thank Hermilio Zarco for his help with the experimental setup and DGAPA and the ICYT-DF for their financial support.

## References

[1] O. Peña, U. Pal, L. Rodríguez-Fernández, A. Crespo-Sosa, J. Opt, Soc. Am. B 25 (2008) 1371.

[2] B.L. Cushing, V.L. Kolesnichenko, C.J. O'Connor, Chem. Rev. 104 (2004) 3893.

[3] R.D. Averitt, S.L. Westcott, N.J. Halas, J. Opt, Soc. Am. B 16 (1999) 1824.

[4] A.M. Schwartzberg, T.Y. Olson, Ch.E. Talley, J.Z. Zhang, J. Phys, Chem. B 110 (2006) 19935.

[5] L.D. Zhang, G.W. Meng, F. Phillipp, Mater. Sci. Eng.: A 286 (2000) 34.

[6] J. Jang, B. Lim, J. Lee, and T. Hyeon, Chem. Commun., 83–84 (2001).

[7] W. Kratschemer, l.D. Lamb, K. Fostiropoulos, D.R. Huffman, Nature 347 (1990) 354.

[8] K. Dai, L. Shi, J. Fang, Y. Zhang, Mater. Sci. Eng.: A 465 (2007) 283.

[9] T. Oku, T. Kusunose, T. Hirata, N. Sato, R. Hatakeyama, K. Niihara, K. Suganuma, Diamond and Related Materials 9 (2000) 911.

[10] P.V. Adhyapak, P. Karandikar, K. Vijayamohanan, A.A. Athawale, A.J. Chandwadkar, Mater. Lett. 58 (2004) 1168.

[11] X.M. Sun, Y.D. Li, Adv. Mater. 17 (2005) 2626.

[12] L.B. Luo, S.H. Yu, H.S. Qian, T. Zhou, J. Am, Chem. Soc. 127 (2005) 2822.

[13] V. Rodríguez-Iglesias, O. Peña, H.G. Silva-Pereyra, L. Rodríguez-Fernández, G. Kellermann, J.C. Cheang-Wong, A. Crespo-Sosa, and A. Oliver, Appl. Phys. B, in press.

[14] P.C. Waterman, Phys. Rev. D 3 (1971) 825.

[15] M.I. Mishchenko, L.D. Travis, Opt. Commun. 109 (1994) 16.

[16] M.I. Mishchenko, L.D. Travis, A. Macke, Appl. Opt. 35 (1996) 4927.

[17] D.J. Wielaard, M.I. Mishchenko, A. Macke, B.E. Carlson, Appl. Opt. 36 (1997) 4305.

[18] A. Quirantes, J. of Quant. Spectr. & Rad. Transf. 92 (2005) 373.

[19] O. Peña, L. Rodríguez-Fernández, V. Rodríguez-Iglesias, G. Kellermann, A. Crespo- Sosa, J.C. Cheang-Wong, H.G. Silva-Pereyra, J. Arenas-Alatorre, A. Oliver, Appl. Opt. 48 (2009) 566.

[20] S. Muhl, F. Maya, S. Rodil, E. Camps, M. Villagrán, A. García, Thin Solid Films 433 (2003) 50.

[21] S. Muhl, F. Maya, S. Rodil, G. Gonzalez, E. Camps, L. Escobar-Alarcon, M. Espinosa-Pesqueira, J. of Optoelect. and Adv. Mat. 7 (2005) 231.

[22] M.I. Mishchenko, L.D. Travis, A.A. Lacis, Scattering, absorption, and emission of light by small particles, Cambridge University Press, U.K., 2002.

[23] P.B. Johnson, R.W. Christy, Phys. Rev. B 6 (1972) 4370.

[24] A.C. Ferrari, A. Libassi, B.K. Tanner, V. Stolojan, J. Yuan, L.M. Brown, S.E. Rodil, B. Kleinsorge, J. Robertson, Phys. Rev. B. 62 (2000) 11089.

[25] A.L. Patterson, Phys. Rev. 56 (1939) 978.

[26] C. Noguez, Opt. Mater. 27 (2005) 1204.

[27] M.I. Mishchenko, D.W. Mackowski, Opt. Lett. 19 (1994) 1604.

[28] D.W. Mackowski, J. Opt, Soc. Am. A 11 (1994) 2851.